Formation of magnetic domains and domain walls in epitaxial $Fe_3O_4(100)$ elements

M. Fonin,* C. Hartung, U. Rüdiger, and M. Kläui†

Fachbereich Physik, Universität Konstanz, 78457 Konstanz, Germany

D. Backes‡ and L. Heyderman

Laboratory for Micro- and Nanotechnology,

Paul Scherrer Institut, 5232 Villigen PSI, Switzerland

F. Nolting and A. Fraile Rodríguez

Swiss Light Source, Paul Scherrer Institut, 5232 Villigen PSI, Switzerland

(Dated: November 5, 2010)

Abstract

Magnetic domains and domain walls in epitaxial $Fe_3O_4(100)$ elements (rings and wires) are imaged using magnetic force microscopy and photoemission electron microscopy. We show that the interplay between the four-fold magnetocrystalline anisotropy and the shape determines the equilibrium domain structure. Domain walls with a characteristic zig-zag structure are observed in $Fe_3O_4(100)$ elements initially magnetized along one of the magnetocrystalline hard axes. We attribute the formation of zig-zag domain walls to the competition of the four-fold magnetocrystalline anisotropy, the exchange and dipolar coupling. A direct correlation between the wire width and the spin structure of zig-zag domain walls is found.

PACS numbers: 57.60.Ch, 72.80.Ga, 85.70.Kh

*Electronic address: mikhail.fonin@uni-konstanz.de

†Also at: Laboratory of Nanomagnetism and Spin Dynamics, Ecole Polytechnique Fédérale de Lausanne (EPFL), 1015 Lausanne, Switzerland; SwissFEL, Paul Scherrer Institut, 5232 Villigen PSI, Switzerland; mathias.klaeui@magnetism.ch

‡Also at Fachbereich Physik, Universität Konstanz, 78457 Konstanz, Germany

Nanoscale ferromagnetic elements play a key role in the emerging field of spintronics, which takes advantage of the electron spin for the realization of future high-speed, high-density, and nonvolatile devices. The performance of such devices, based either on magnetoresistance (MR) effects, [1–4] domain wall (DW) magnetoresistance [5, 6] or current-induced domain wall motion (CIDM), [7–9] can be enhanced using ferromagnetic materials exhibiting a high degree of spin polarization. Of particular interest are so-called half-metallic ferromagnets, compounds that are metallic for one spin component while insulating for the other spin component, thus leading to 100 % spin polarization at the Fermi energy (E_F). In this context magnetite (Fe_3O_4) is a very important material combining a high Curie temperature $T_C = 851$ K with a high spin polarization of up to -80 % at room temperature. [10, 11] Until now, magnetic properties of mesoscopic Fe_3O_4 elements have not been extensively investigated, and first experiments have recently been reported showing extraordinarily high MR values in Fe_3O_4 wires with nanoconstrictions. [12]

For both applications and understanding of fundamental physical effects related to the high spin polarization, such as DW magnetoresistance effects and CIDM, controlled magnetization configurations have to be obtained. This is only possible in magnetic micro- or nanostructures, where the magnetic properties can be tailored by engineering the geometry. Some of the most promising geometries are rings [13] or wires, where simple and reproducible domain wall structures are obtained and which might prove useful for applications such as in the racetrack memory device based on DW propagation. [14] Prior to being able to use Fe_3O_4 micro- or nanostructures for any kind of device, a detailed understanding of the magnetic states including the DW spin structures that result from the interplay of the shape anisotropy and the intrinsic magnetocrystalline anisotropy has to be obtained. [15]

In this paper, we investigate magnetization configurations with x-ray magnetic circular dichroism photoemission microscopy (XMCD-PEEM) and magnetic force microscopy (MFM) as well as their correlation to the geometry in epitaxial $Fe_3O_4(100)$ elements. We show that, in contrast to the usual transverse and vortex DWs in 3*d* metals, [15] a distinctly different DW type can be observed due to the interplay between the magnetocrystalline anisotropy, the exchange and dipolar coupling in epitaxial $Fe_3O_4(100)$ elements. To determine the influence of the shape, we image the magnetization configuration in structures with varying width.

High quality 40 -50 nm thick $Fe_3O_4(100)$ films were prepared by molecular beam epitaxy

(MBE) evaporation of Fe on MgO(100) substrates in an O_2 atmosphere. [11, 16] Figure 1 (a) shows the magnetic moment versus temperature curves of a 50-nm-thick $Fe_3O_4(100)$ film. The transition temperature of 120 K together with the sharpness of the transition indicate the high quality of prepared Fe_3O_4 films. The hysteresis loops of an epitaxial 50 nm thick Fe_3O_4 film measured by SQUID magnetometry along two different in-plane crystallographic directions ($[0\bar{1}1]$ and [001]) are presented in Fig. 1 (b). The shapes of the hysteresis loops measured along the [011] and [010] directions were identical to those measured in the $[0\bar{1}1]$ and [001] directions, respectively, pointing to an in-plane four-fold symmetry which reflects the cubic anisotropy of the bulk material. From the comparison of the hysteresis loops along the [001] and the $[0\bar{1}1]$ crystallographic directions, it can be concluded that the in-plane easy axes lie along the in-plane $< 011 >$ directions. The anisotropy constant K_1 as well as the value of saturation magnetization M_S could be calculated from the measured hysteresis loops. Within the error bars the measured values are consistent with the literature values $M_S = 4.8 \cdot 10^5\ A/m$ [17] and $K_1 = -1.1 \cdot 10^4\ J/m^3$ [18].

Fe_3O_4 structures were fabricated from 40 nm thick films by focussed ion beam or argon ion milling using a Cr hard mask defined by electron beam lithography and a lift-off process. Structures consisting of either arrays of rings with varying outer diameter, D, and line width, W, or zig-zag lines were prepared. To image the magnetization configurations XMCD-PEEM at the Fe $L_{2,3}$ edge as well as MFM are used. MFM measurements on the Fe_3O_4 structures were performed at RT by using a Digital Instruments MULTIMODE™ scanning probe microscope. The magnetic contrast is separated from the topographical features by scanning each line twice in a two-step tapping/lift mode. Cobalt coated low moment POINTPROBE-PLUS® Silicon-SPM-Sensors from Nanosensors™ were used as cantilevers in all experiments.

In Fig. 2, a high resolution XMCD-PEEM image (a) of a Fe_3O_4 ring structure (D = 10 μm, nominal width W = 1135 nm) initially magnetized along one of the magnetocrystalline hard axes (the [001] direction) is compared with a simulated magnetization configuration obtained from micromagnetic calculations (b). The black (white) contrast in the XMCD-PEEM image [Fig. 2 (a)] reflects the horizontal component of the in-plane magnetization direction pointing to the left (right). The main difference to the magnetization configurations of polycrystalline $3d$ metal rings is that here the in-plane magnetization deviates **from** the direction given by the shape of the structure. Instead of following the ring perimeter, the magnetization is

divided into four domains. Within each of the domains, the magnetization points along one of the in-plane magnetocrystalline easy axes (the crystallographic directions are marked in the center of Fig. 2). In the neighboring segments of the ring, the magnetization vectors are perpendicular to each other, causing two 90° DWs at the right and the left side of the ring (marked with A). The configuration resembles the onion state magnetic configuration observed in $3d$ metal rings. [13] In this state the Fe_3O_4 ring structure contains characteristic head-to-head and tail-to-tail DWs, indicated by the change from black to white (and vice versa) at the top and bottom of the ring (the position of the tail-to-tail DW at the top is marked with B). In contrast to the transverse or vortex DWs observed in permalloy, [15, 19] the head-to-head (tail-to-tail) DWs in Fe_3O_4 exhibit a zig-zag shape (see e.g. the tail-to-tail DW marked with B).

In order to understand the remanent magnetic states observed in Fe_3O_4 rings, we perform micromagnetic simulations of the equilibrium state at remanence. Micromagnetic simulations were carried out using the object oriented micromagnetic framework (OOMMF) code. [20] The Fe_3O_4 parameters used were $M_S = 4.8 \cdot 10^5\ A/m$ [17] for the saturation magnetization, and $A = 1.2 \cdot 10^{-11}\ J/m$ [18] for the exchange stiffness. The value of the anisotropy constant was set to $K_1 = -1.1 \cdot 10^4\ J/m^3$. [18] A cell size of 10 nm was used which is similar to the exchange length. A damping parameter $\alpha = 0.1$ was chosen. For the calculation, the magnetization was first saturated along one of the magnetocrystalline hard axes and then was allowed to relax without any applied field. The equilibrium state at remanence obtained from the micromagnetic simulations for a ring structure with $D = 5\,\mu$m and $W = 1135$ nm is shown in Fig. 2 (b). The gray scale for the magnetization directions is chosen to be identical with the XMCD-PEEM image contrast in (a). The micromagnetic simulation reproduces the four domain structure measured by XMCD-PEEM extremely well, exhibiting two 90° DWs and two zig-zag DWs. The four domain structure is a consequence of the strong four-fold in-plane magnetocrystalline anisotropy of $Fe_3O_4(100)$ films. The magnetocrystalline anisotropy favors alignment of the magnetization along the easy axes, i.e. along the in-plane $< 011 >$ crystallographic directions. The formation of the observed zig-zag DW structure in epitaxial Fe_3O_4 rings is the result of the energetic compromise between the four-fold magnetocrystalline anisotropy, the exchange and dipolar coupling. In a ring structure, two neighboring domains meet at 90° due to the strong magnetocrystalline anisotropy and the separating DW develops a characteristic zig-zag shape to reduce the magnetic charge den-

sity compared to a straight wall, which would have a larger magnetic charge concentration. Thus increasing the zig-zag angle, the magnetic charge density decreases at the expense of the wall surface.

Further investigation of the domain structure was performed by MFM. Fig. 2 (c) shows an MFM image of an Fe_3O_4 ring ($D = 5\,\mu$m, nominal width $W = 1135\,$nm). The initial magnetization direction is the same as for the simulation and the XMCD-PEEM image. In (d) the formation of the MFM contrast is visualized schematically. Since the magnetization does not follow the shape of the ring exactly but points along the directions of the magnetocrystalline easy axes, in the MFM image strongest contrast can be seen at the inner and the outer rim of the structure. The pronounced black and white areas at the top and the bottom of the ring result from the head-to-head/tail-to-tail DWs, while the contrast change from white to black at the left and right outer rim of the structure is caused by the 90° DWs (and correspondingly, the contrast change from black to white at the inner rim of the ring). The MFM image is consistent with the domain structure determined by the XMCD-PEEM measurement and by the OOMMF simulation. However, it is not possible to deduce the exact DW spin structure from the MFM image, so that the direct XMCD-PEEM imaging is key for the exact determination the of magnetic configurations.

If the ring microstructures are initially magnetized along one of the easy axes a modification of the onion state can be observed. In Fig. 3, an MFM image of an Fe_3O_4 ring ($D = 5\,\mu$m, nominal width $W = 530\,$nm) is presented compared with the corresponding OOMMF simulation. Now, in addition to the head-to-head and the tail-to-tail domain wall, four 90° reorientations arising from the influence of magnetocrystalline anisotropy can be seen. The ring structure is divided into six different sections within which the magnetization follows the directions of the easy axes, and dark and bright areas are observed at the inner and outer rim of the ring structure. In contrast to the situation arising in the case of initial magnetization along the hard axis, the head-to-head and tail-to-tail walls are now true 180° transverse domain walls. In the MFM image, this means that those parts of the rim which are directly adjacent to the walls do not show magnetic contrast. The 90° spin reorientation again correspond to contrast changes at the rim from black to white (or vice versa).

For experiments involving DW displacements, ring structures are not ideally suited since they exhibit the additional 90° DWs. In $3d$ metals, the wire geometry has already proven to be suitable for CIDM experiments [7, 9, 15] and so next we pattern Fe_3O_4 into a wire

geometry. An XMCD-PEEM image of the Fe_3O_4 wires of various widths is shown in **Fig. 4**. Initially the wires were magnetized along a magnetocrystalline hard axis, resulting in a multi-domain state with head-to-head (tail-to-tail) DWs located at the kinks. The DWs are zig-zag walls similar to those already found in the Fe_3O_4 rings described above. The zig-zag DW structure is observed to depend on the width of the wire. The wider the wire, the more complicated the wall structure showing more zig-zags. Such DW structures evolve in wider wires because the DW can decrease the charge density by a repeated zig-zag folding. The complicated zig-zag DW structure is not favourable for CIDM experiments, since this extra degree of freedom could lead to changes in the wall structure complicating the wall motion so narrow wires will have to be used. An additional problem arises from the fact that for wires angles are different from 90°, thus leading to an offset between the magnetization vectors and the wire segment direction, i.e. the magnetization does not exactly follow the shape of the structure. So here care has to be taken when choosing the direction of the wire to align the structure with the magnetocrystalline easy axes.

In conclusion, we found that the in-plane four-fold magnetocrystalline anisotropy dominates the magnetic structure in epitaxial $Fe_3O_4(100)$ elements, leading to domain configurations substantially different from those observed in polycristalline $3d$ metal structures with the same geometry and size. For the structures initially magnetized along one of the magnetocrystalline hard axes, the magnetic state correspond to a four domain configuration typical of systems with cubic anisotropy. We observe that the in-plane magnetization does not follow the exact shape of the $Fe_3O_4(100)$ structures because of the interplay between the shape anisotropy and the four-fold magnetocrystalline anisotropy that favors alignment of the magnetization along the easy axes, i.e. along the in-plane $< 011 >$ crystallographic directions. We show that the four-fold magnetocrystalline anisotropy combined with the shape of the element gives rise to characteristic zig-zag DWs which are the result of magnetic charge density minimization by a zig-zag folding. By reducing the wire width the spin structure of the domain wall becomes simpler and better defined so that narrow wires of this highly spin-polarized material are promising candidates for experiments involving DW propagation induced by fields or currents.

ACKNOWLEDGMENTS

This work was supported by the Deutsche Forschungsgemeinschaft (SFB 767, KL1811), the European Research Council (ERC-2007-StG 208162 MASPIC), the Swiss National Science Foundation and the Landesstiftung Baden-Württemberg. Part of this work was performed at the Swiss Light Source, Paul Scherrer Institut, Villigen, Switzerland.

---

[1] M. N. Baibich, J. M. Broto, A. Fert, F. Nguyen Van Dau, F. Petroff, P. Etienne, G. Creuzet, A. Friederich, and J. Chazelas, Phys. Rev. Lett. **61**, 2472 (1988).

[2] G. Binasch, P. Grünberg, F. Saurenbach, and W. Zinn, Phys. Rev. B **39**, 4828 (1989).

[3] T. Miyazaki and N. Tezuka, J. Magn. Magn. Mater. **139**, L231 (1995).

[4] J. S. Moodera, L. R. Kinder, T. M. Wong, and R. Merservey, Phys. Rev. Lett. **74**, 3273 (1995).

[5] A. D. Kent, J. Yu, U. Rüdiger, and S. S. P. Parkin, J. Phys.: Condens. Matter **13**, R461 (2001).

[6] M. Kläui, C. A. F. Vaz, J. Rothman, J. A. C. Bland, W. Wernsdorfer, G. Faini, and E. Cambril, Phys. Rev. Lett. **90**, 097202 (2003).

[7] A. Yamaguchi, T. Ono, S. Nasu, K. Miyake, K. Mibu, and T. Shinjo, Phys. Rev. Lett. **92**, 077205 (2004).

[8] M. Kläui, C. A. F. Vaz, J. A. C. Bland, W. Wernsdorfer, G. Faini, E. Cambril, L. J. Heyderman, F. Nolting, and U. Rüdiger, Phys. Rev. Lett. **94**, 106601 (2005).

[9] M. Kläui, P.-O. Jubert, R. Allenspach, A. Bischof, J. A. C. Bland, G. Faini, U. Rüdiger, C. A. F. Vaz, L. Vila, and C. Vouille, Phys. Rev. Lett **95**, 026601 (2005).

[10] Yu. S. Dedkov, U. Rüdiger, and G. Güntherodt, Phys. Rev. B **65**, 064417 (2002).

[11] M. Fonin, Yu. S. Dedkov, R. Pentcheva, U. Rüdiger, and G. Güntherodt, J. Phys.: Condens. Matter **19**, 315217 (2007).

[12] O. Céspedes, S. M. Watts, J. M. D. Coey, K. Dörr, and M. Ziese, Appl. Phys. Lett. **87**, 083102 (2005).

[13] M. Kläui, C. A. F. Vaz, L. Lopez-Diaz, and J. A. C. Bland, J. Phys.: Condens. Matter **15**, R985 (2003).

[14] S. S. P. Parkin, M. Hayashi, and L. Thomas, Science, **320**, 190 (2008).

[15] M. Kläui, J. Phys.: Condens. Matter **20**, 313001 (2008).

[16] M. Fonin, R. Pentcheva, Yu. S. Dedkov, M. Sperlich, D. V. Vyalikh, M. Scheffler, U. Rüdiger, and G. Güntherodt, Phys. Rev. B **72**, 104436 (2005).

[17] S. Kale, S. Bhagat, S. Lofland, T. Scabarozi, S. Ogale, A. Orozco, S. Shinde, T. Venkatesan, B. Hannoyer, B. Mercey, and W. Prellier, Phys. Rev. B **64**, 205413 (2001).

[18] M. Ziese, R. Höhne, P. Esquinazi, and P. Busch, Phys. Rev. B **66**, 134408 (2002).

[19] R. D. McMichael and M. J. Donahue, IEEE Trans. Magn. **33**, 4167 (1997).

[20] The Object Oriented MicroMagnetic Framework (OOMMF) project, ITL/NIST. For details see, http://math.nist.gov/oommf

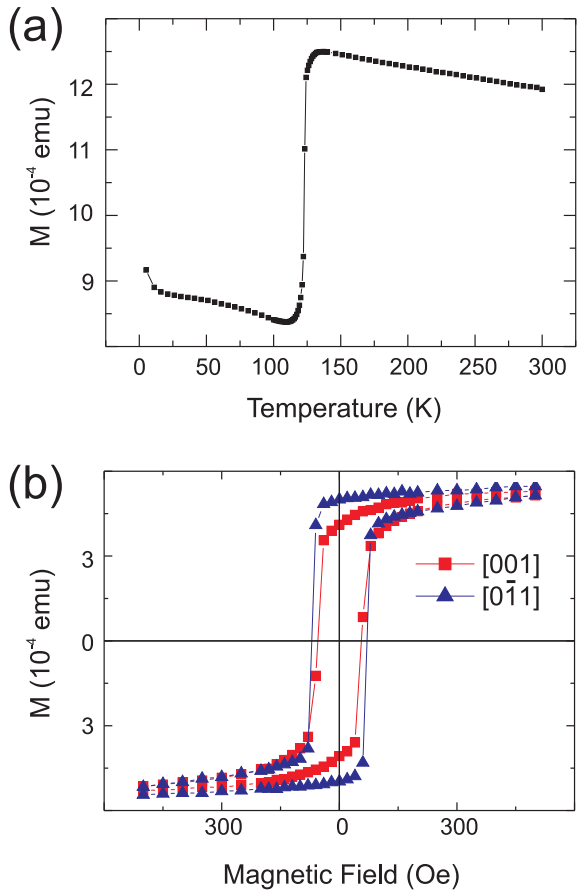

FIG. 1: (Color online) (a) Magnetic moment of a 50-nm-thick epitaxial $Fe_3O_4(100)$ film on MgO(100) as a function of temperature. The curve exhibits a sharp step at 120 K corresponding to the Verwey transition. (b) Hysteresis loops along different in-plane crystallographic axes of the $Fe_3O_4(100)$/MgO(100) sample at 300 K.

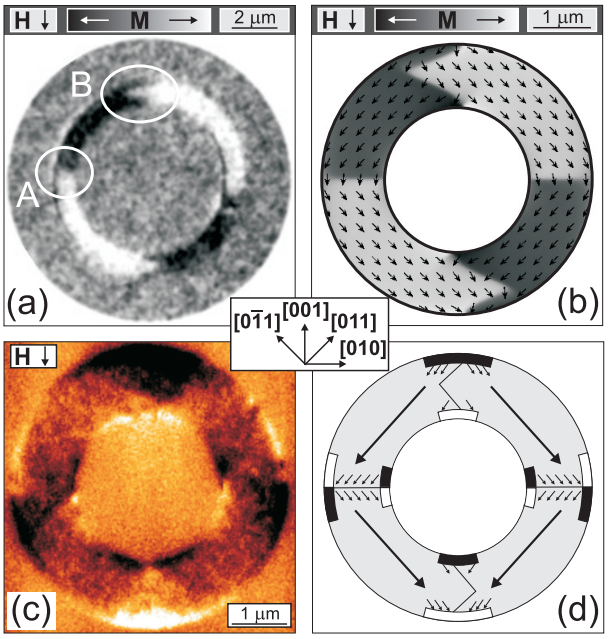

FIG. 2: (Color online) (a) High resolution XMCD-PEEM image of a Fe_3O_4 ring ($D = 10\,\mu$m, nominal width $W = 1135\,$nm) at zero-field. 90° DWs are visible in the image (marked with A). A tail-to-tail zig-zag DW (marked with B) as well as a head-to-head zig-zag DW at the opposite side of the ring are also present. Black and white contrasts correspond to the magnetization pointing to the left and right, respectively. (b) Simulated magnetization orientation obtained from the micromagnetic calculation for the Fe_3O_4 ring ($D = 5\,\mu$m, $W = 1135\,$nm) in the remanent state after saturation. (c) Analogous MFM image of the Fe_3O_4 ring ($D = 5\,\mu$m, nominal width $W = 1135\,$nm). In (d) the MFM contrast is visualized schematically. The samples were initially magnetized with a field H along a hard axis (the [001] direction), as indicated by the arrow in the upper left corner of each image. The in-plane crystallographic directions are marked in the center of the figure.

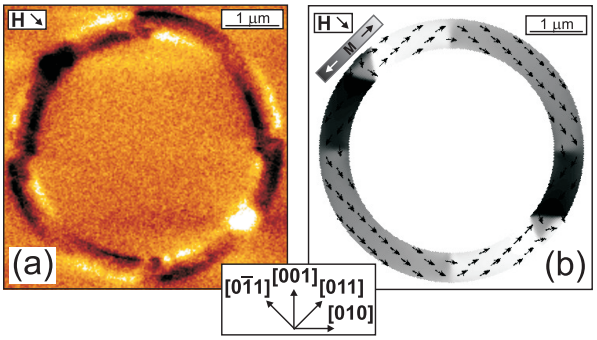

FIG. 3: (Color online) (a) MFM image of the Fe_3O_4 ring ($D = 5\,\mu$m, nominal width $W = 530\,$nm) together with the corresponding OOMMF simulation results (b), initially magnetized along the easy axis. The in-plane crystallographic directions are marked at the bottom of the figure.

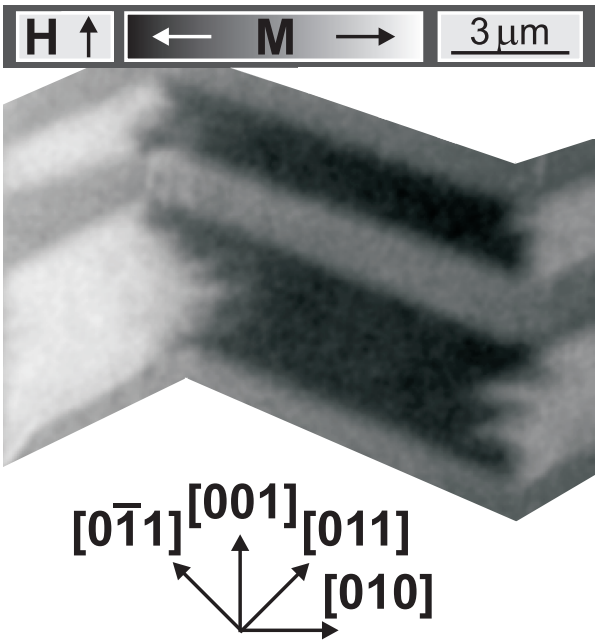

FIG. 4: (Color online) XMCD-PEEM image of Fe_3O_4 wires of different line widths ($W = 2000\,$nm top wire, $W = 3500\,$nm bottom wire). The sample was initially magnetized with a field H along a hard axis (the [001] direction), as indicated by the arrow in the upper left corner of each image.